九州大学大学院総合理工学報告
第 46 巻 第 1 号 1-6 頁 令和 6 年 9 月

Engineering Sciences Reports, Kyushu University
Vol. 46, No. 1, pp. 1-6, SEP, 2024

Photon-photon resonance phenomenon in active multimode interferometer laser as Fabry-Perót laser

He XIAO*1, Yudai KAWANO*1, Haisong JIANG*2†,
and Kiichi HAMAMOTO*2
†E-mail of corresponding author: jiang.haisong.447@m.kyushu-u.ac.jp

(Received January 10, 2024, accepted March 11, 2024)

Photon-photon resonance (PPR) has attracted attention for its capability to extend modulation speed of directly modulated laser (DML). PPR is phenomenon resulted from the interference of two lasing modes. For the general Fabry-Perót (F-P) lasers, though multiple wavelengths exist, it has been considered as a structure that could not explore PPR phenomenon. This is because the lasing modes in F-P laser are all orthogonal. Active-MMI (multimode interferometer) laser as a F-P laser, however, has been observed the PPRs experimentally. In this paper, the existence of PPR in active-MMI LD has been confirmed theoretically. This calculation method provides a way to evaluate the location of PPR in the design.

Key words: *PPR, DML, modulation bandwidth, Fabry-Perót lasers*

1. Introduction

Directly modulated laser (DML) is expected as one of the suitable data-transmitters especially in computing system [1]. The directly modulated laser's modulation bandwidth in general, is restricted by so-called relaxation oscillation frequency (or carrier photon resonance (CPR) frequency) [2]. Lots of efforts have been paid to extend DML modulation bandwidth [3-10]. One possible way to overcome the restriction of relaxation oscillation is to utilize PPR (photon-photon resonance) which realizes higher frequency resonance compared to CPR [11-25]. From the previous works, all the configurations that have been utilized to exploit PPR phenomenon share the common grating. All the reported DMLs with PPR are those distributed Bragg reflector (DBR) lasers or distributed feedback (DFB) lasers. PPR is known as a resonance caused by the interaction between two lasing modes. PPR phenomenon is not able to be observed in Fabry-Perót (F-P) laser because of the mode orthogonality [26-27] among the longitudinal modes. In 2017, however, the existence of the PPR phenomenon in F-P laser has been proved [28-32]. By applying active-multimode interferometer (MMI) laser, the plural PPRs phenomenon was observed which contradicts the principle.

In this paper, the mode orthogonality in F-P laser will be clarified. Then, non-orthogonality in active-MMI for multiple PPRs is explained. Since active-MMI laser naturally accesses multiple waveguides, different oscillators exist that non-orthogonal mode do exist in active-MMI laser which provides the possibility to exploit PPR.

2. Non-orthogonality in active-MMI laser diode

To explain the mode orthogonality in Fabry-Perót laser, longitudinal lasing modes in F-P laser is clarified first [33]. Figure 1 is a schematic diagram of F-P laser. The F-P cavity whose length is L, is filled with semiconductor material with a refractive index n_r. At the both ends, there are two reflection mirrors with reflective index R_1 and R_2. The electromagnetic wave that exists in this cavity is expressed in

*1 Department of Applied Science for Electronics and Materials. Graduate Student
*2 Department of Advanced Energy Science and Engineering.

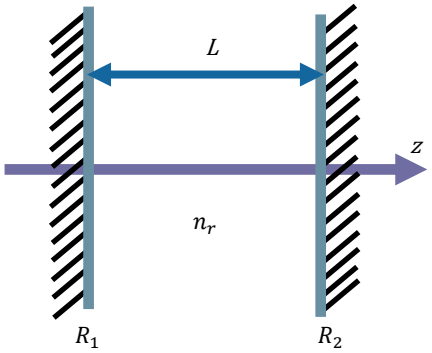

Fig. 1 Schematic diagram of Fabry-Perót laser.

$$E = exp\left[\frac{i2\pi n_r z}{\lambda_0}\right] exp[(g-\alpha_i)z] \quad (1)$$

In the expression, λ_0 is the wavelength in free space. α_i is the internal loss coefficient. g is gain coefficient. The condition for the existence of an electromagnetic wave is that, when this electromagnetic wave is reflected to its origin, its amplitude has to be equal to the starting value. For the lasing modes, the electronic fields are

$$E_m = A_m e^{jm\left(\frac{z}{L}\right)\pi} \quad (2)$$

A_m is the amplitude. L is the cavity length. m is the order of the longitude mode. The PPR phenomenon enhance the modulation bandwidth as the interaction between two modes increase. The strong lasing mode is called main mode. The weak lasing mode is called sub mode. The coupling efficiency η_z between main and sub modes is important to PPR phenomenon. The coupling efficiency between different modes is explained as the spatial overlap between different modes as shown in Eq. (3).

$$\eta_z = \int_0^{2L} E_{main}\, E_{sub}\, dz \quad (3)$$

As the lasing modes in Fabry-Perót laser originate from Fabry-Perot resonance in the same cavity, all the longitudinal lasing modes are orthogonal to each other. In this case, the coupling efficiency η_z, which is expressed in Eq. (3) is calculated as below:

$$\eta_z = \int_0^{2L} A_{main} e^{jm_{main}\left(\frac{z}{L}\right)\pi}\ A_{sub} e^{jm_{sub}\left(\frac{z}{L}\right)\pi} dz = \frac{A_{main}A_{sub}}{j\pi\left(\frac{m_{main}}{L}+\frac{m_{sub}}{L}\right)} e^{j(m_{main}+m_{sub})\frac{z}{L}\pi}\Big|_0^{2L} = 0 \quad (4)$$

And the coupling efficiency η_z is to be zero. The result means that all the lasing modes in the Fabry-Perót cavity are orthogonal and thus any PPR phenomenon is not caused any more. According to the PPR rate equation [31],

$$\frac{dS_1(t)}{dt} = G_1[N(t)-N_{th}]\times[S_1(t)]$$

$$\frac{dS_2(t)}{dt} = G_2[N(t)-N_{th}]\times[S_2(t)] + 2\kappa\sqrt{[(S_1(t)]\times[S_2(t)]}cos\phi(t)$$

$$\frac{d\phi(t)}{dt} = \frac{\alpha}{2}[G_2(N(t)-N_{th})] - \kappa\frac{S_1(t)}{S_2(t)}sin\,\phi(t) - \Delta\omega$$

$$\frac{dN(t)}{dt} = J - \frac{N(t)}{\tau_r} - G_1[N(t)-N_{tr}]\times[S_1(t)] - G_2[N(t)-N_{tr}]\times[S_2(t)] \quad (5)$$

S_1, S_2, are the photon number of two lasing modes in laser diode. $N(t)$ and N_{th}, N_{tr}, α are carrier number and the threshold carrier number, transparency carrier number, linewidth-enhancement factor, respectively. τ_r is carrier lifetime. G_1, G_2 is the gain coefficient of the main lasing mode and sub-lasing mode. $\Delta\omega$ is the frequency difference between two lasing modes. J is the current injection. κ is the coupling parameter. In the F-P lasers, because of the orthogonality of all lasing modes, there is no interaction between different modes. The interaction terms related to coupling parameter κ in Eq. (5) are zero that the rate equations with PPR degenerate to the general rate equations without PPR. Thus, the PPR phenomenon is rarely observed in F-P lasers.

The configuration of active-MMI laser [32] reported to observe multiple PPRs is shown in Fig. 2.

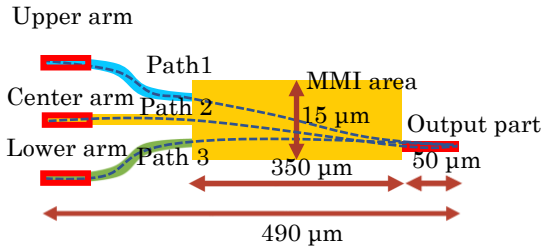

Fig. 2 Schematic diagram of active-MMI laser.

The situation of Fabry-Perót resonance in active-MMI LD is slightly different from the above-discussed general case of Fabry-Perót LD. Even though in a single device, there are several different light-path inside of the device. There are three parts in this device. In the middle is the MMI areas. The LHS of MMI area are three arm parts, called upper arm, middle arm and lower arm respectively. In the RHS of the MMI area, it is another waveguide working as modulation port. There are three different optical paths named path 1, path 2 and path 3 in that cavity. The coupling efficiency η_z in active-MMI laser diode is

$$\eta_z = \int_0^{2L_{main}} A_{main} e^{jm_{main}\frac{z\pi}{L_{main}}}\ A_{sub} e^{jm_{sub}\frac{z\pi}{L_{sub}}} dz$$

$$= \frac{A_{main}A_{sub}}{j(\frac{\pi m_{1main}}{L}+\frac{\pi m_{sub}}{L})} e^{j\left(\frac{m_{main}}{L_{main}}+\frac{m_{sub}}{L_{sub}}\right)z\pi}\Big|_0^{2L_{main}} \quad (6)$$

As the optical cavity in active-MMI laser diode for different path is different, the coupling efficiency η_z is

$$\eta_z = \frac{A_{main}A_{sub}}{j\pi(\frac{m_{main}}{L_{main}}+\frac{m_{sub}}{L_{sub}})} \times \left(e^{j(2m_{main}+2m_{sub}\frac{L_{main}}{L_{sub}})\pi}-1\right) \neq 0$$

Therefore, non-orthogonal lasing modes exist in active-MMI laser diode. To confirm this path difference in the active-MMI LD shown in Fig. 2, we do simulations by using the FDTD (finite-division time-domain) method [20].

The initial light is injected from three arms respectively. We monitored the phase of the propagated light at the single output waveguide end. If the path length is the same among three different injection conditions, the achieved phase as a function of wavelength must be completely matched to each other. The simulation results are shown in Fig. 3 (a1). The phase conditions for each path are different from each other. This confirms our thought that there are non-orthogonal modes in active-MMI LD.

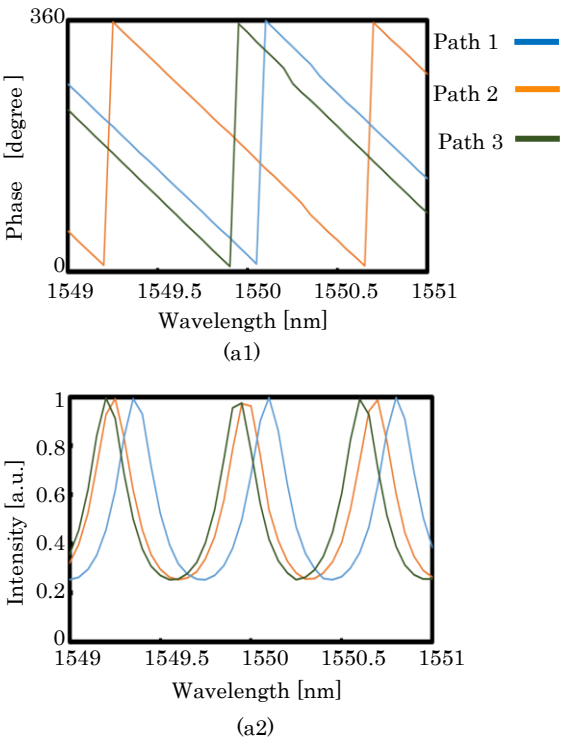

Fig. 3 (a1) Phase in each path in active-MMI laser;
(a2) Transmittance of each arm in active-MMI laser.

From Fig. 3 (a2), the wavelength whose transmittance is equal to 1 are modes that may exist in the path. Hence, the effective optical path length for each path. For each path, those wavelengths whose transmittance is equal to 1 are called λ_{peak}. In the simulation range, there are three λ_{peak} for each path. With the relationship expressed in Eq. (2), the optical path for each path is achieved and shown in Table 1.

Table 1 Optical path for three paths in active-MMI LD.

	λ_{peak1} [nm]	λ_{peak} [nm]	Δλ [nm]	Optical path [μm]
Path 1	1549.35	1550.1	0.75	500.33
Path 2	1549.25	1549.975	0.725	517.52
Path 3	1549.2	1549.925	0.725	517.49

Based on the research on the PPR phenomenon, the spectrum of laser is very important information to confirm the PPR phenomenon. From all the works concentrated on the PPR phenomenon, experimentally, except for the main lasing wavelength, there is another weak lasing wavelength. The location of PPR is derived from

$$f_{ppr} = c(\frac{1}{\lambda_{main}} - \frac{1}{\lambda_{sub}}) \quad (7)$$

where λ_{main} and λ_{sub} are wavelengths for the strong lasing mode and weak lasing mode. c is the light velocity in vacuum. It indicates that the location of PPR is related to the spectrum. Thus, the predictable spectrum will help us to utilize PPR to extend the modulation bandwidth.

3. Spectrum of active-MMI LD

3.1 Simulation results

To get the spectrum, the intensity ratio of each arm has to be clarified. Because of the self-image phenomenon [34], the ratio of optical power from each path is not the same weight in active-MMI LD. As shown in Fig. 4, when the light is injected from the single-end side, the percentage of the power in each path is different. The majority of power is propagated through path 1 which is accessed with the upper arm. The second most power is propagated through path 2 connected to the middle arm. Path 3 related to the lower arm contributes the least to light propagation.

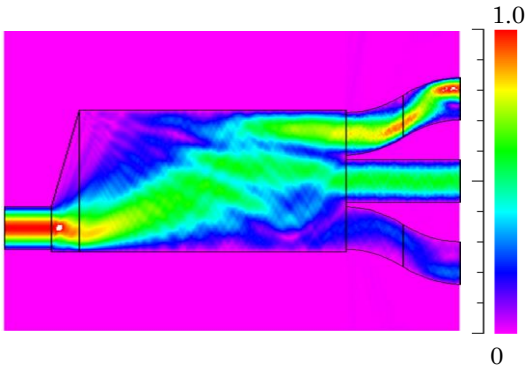

Fig. 4 Intensity ratio of each path in active-MMI laser.

Taking this intensity ratio into account, the transmittance of each arm will be shown in Fig. 5.

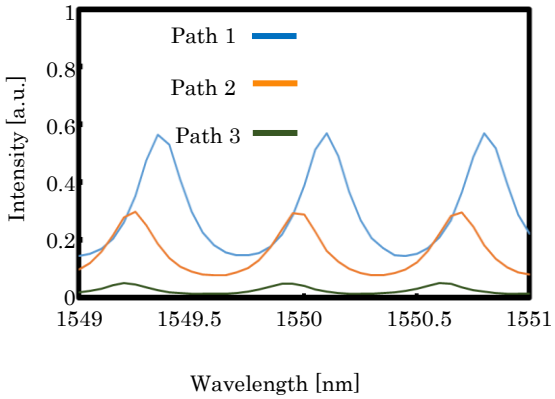

Fig. 5 Transmittance of each arm in active-MMI laser.

It is necessary to clarify that, when this configuration is working as an active device, the lasing mode generated by path 1 may not be the main lasing mode, and the lasing mode related to another path may not be the sub-lasing mode either. This is because all the simulations we carried out did not consider the gain. Thus, it is unclear which one is the main lasing mode until the laser is lasing. However, the wavelength difference does not change. From the wavelength difference, the location of PPR is obtained. The spectrum from passive device simulation is calculated. The results are calculated with the condition that lasers have been through 6 times round-trip times. Figure 6 displays four possible lasing wavelengths 1549.9 nm, 1550.1 nm,1550.6 nm and 1550.7 nm. Though we don't know which one is the main lasing laser, we assume that the laser with wavelength of 1550.1 is the main lasing mode. The details are listed in Table 2. Based on that assumption, there are three possible locations for PPRs. It is 24 GHz, 63 GHz and 75 GHz.

Table 2 The calculated PPR location.

Δλ [nm]	0.2	0.5	0.6
PPR location [GHz]	24	63	75

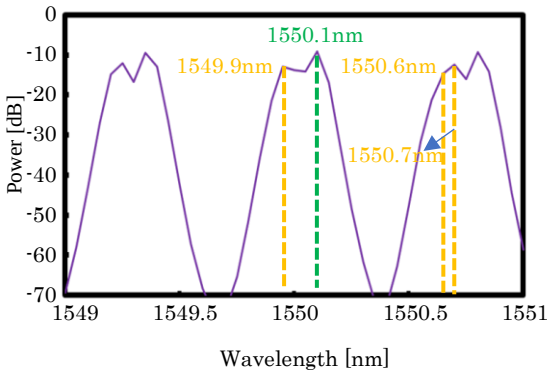

Fig. 6 Calculated spectrum of active-MMI laser.

3.2 Experimental results

The small signal modulation response of the proposed 1×3 active-MMI LD [31] is shown is shown in Fig. 7.

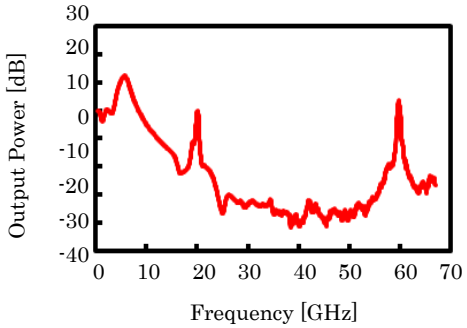

Fig. 7 Calculated spectrum of active-MMI laser.

Two PPRs are observed. One is located at 20 GHz and another is located at 60 GHz. The experiment confirms the prediction of the spectrum. The location of PPR in the experiment is almost in accordance with the theoretical calculation. The reason why there is a difference between theoretical calculation and experiment lies in the lasing condition. The current injection of laser changes the refractive index of the device, which leads to the change of PPR location. From Table 2, there might a PPR located around 75 GHz which is over the range of the experiment equipment.

4. Summary and Conclusion

In this paper, non-orthogonal modes in active-MMI LD are explained. According to the calculation of non-orthogonal modes in active-MMI LD, the theoretical calculation of PPR location in active-MMI LD has been presented. The simulation result is in accordance with the experiment result. This method provides the possibility to calculate the PPR location that benefits the modulation bandwidth enhancement by utilizing PPR.

Acknowledgments

This work was partly supported by Kakenhi #19H02201 and #22H01556.

References

1) Sébastien, R., et al., Optical interconnects for extreme scale computing systems, Parallel Computing, vol. 64, pp. 65-80 (2017).
2) Coldren, L. A., et al., Diode lasers and photonic integrated circuits, John Wiley & Sons, 2012. Chapter 2.
3) R. S. Tucker., High-speed modulation of semiconductor lasers, J. Lightwave Technol., vol.3, no. 6, pp.1180-1192 (1985).
4) Haglund, E., et al., 30 GHz bandwidth 850 nm VCSEL with sub-100 fJ/bit energy dissipation at 25-50 Gbit/s, Electron. Lett., vol. 51, no.14, pp. 1096-1098 (2015).
5) Westbergh, P., et al., High-speed 850 nm VCSELs with 28 GHz modulation bandwidth operating error-free up to 44 Gbit/s, Electron. Lett., vol. 48, no. 18, pp. 1145-1147 (2012).
6) Fedor, Z., et al., High speed data transmission using directly modulated microdisk lasers based on InGaAs/GaAs quantum well-dots, Opt. Lett., vol. 44, no. 22, pp. 5442-5445 (2019).
7) Haglund, E., et al., High-speed 850 nm VCSEL with 30 GHz modulation bandwidth, Proceedings of 2015 European Conference on Lasers and Electro-Optics- European Quantum Electronics Conference, paper CB_2_4 (2015).
8) Wood. T. H., et al., High-speed optical modulation with GaAs/GaAlAs quantum wells in a p-i-n diode structure, Appl. Phys. Lett., vol.44, no.1, pp.16-18 (1984).
9) Zhixin, L., Slavík, R., Optical injection locking: From principle to applications, J. Lightwave Technol., vol. 38, no. 1, pp. 43-59 (2020).
10) Sun. C., et al., Modulation characteristics enhancement of monolithically integrated laser diodes under mutual injection locking, J. Sel. Top. Quantum Electron., vol. 21, no. 6, pp. 628-635 (2015).
11) Matsui. Y., et al., 30-GHz bandwidth 1.55-μm strain-compensated InGaAlAs-InGaAsP MQW laser, Photon. Technol. Lett., vol. 9, no. 1, pp. 25-27 (1997).
12) Zhao. W., et al., Modulation bandwidth enhancement of monolithically integrated mutually coupled distributed feedback laser, Appl. Sci., vol. 10, no. 12, pp. 4375 (2020).
13) Reithmaier. J.P., et al., Modulation speed enhancement by coupling to higher order resonances: A road towards 40 GHz bandwidth lasers on InP, Proceedings of the International Conference on Indium Phosphide and Related Materials, pp. 118-123 (2005).
14) Kreissl J., et al., Up to 40-Gb/s directly modulated laser operating at low driving current: buried-heterostructure passive feedback laser (BH-PFL), Photon. Technol. Lett., vol. 24, no.5, pp. 362-364 (2012).
15) Matsui. Y., et al., 55 GHz Bandwidth distributed reflector laser, J. Lightwave Technol., vol. 35, no.3, pp. 397-403 (2017).
16) Mohrle, M., et al., Detuned grating multisection-RW-DFB lasers for high-speed optical signal processing, J. Sel. Top. Quantum Electron., vol. 7, no.3, pp. 217-223 (2001).
17) Mao, Y., et al., Modulation bandwidth enhancement in distributed reflector laser based on identical active layer approach, Photonics J., vol. 10, no.3, pp. 1-8 (2018).
18) Kreissl, J., et al., 40 Gbit/s directly modulated passive feedback laser with complex-coupled DFB section. Proceedings of the 33rd European Conference and Exhibition of Optical Communications, Paper Tu.1.D.6, (2008).
19) Chacinski, M., Schatz, R., Impact of losses in the Bragg section on the dynamics of detuned loaded DBR lasers, J. Quantum Electron., vol. 46, no. 9, pp. 1360-1367 (2010).
20) Yamamoto, T., et al., Uncooled 40-Gbps direct modulation of 1.3-μmwavelength AlGaInAs distributed reflector lasers with semi-insulating buried-heterostructure, Proceedings of 22nd IEEE Int. Semicond. Laser Conf., Paper ThB3 (2010).
21) Tomkos, I., et al., Extraction of laser rate equations parameters for representative simulations of metropolitan-area transmission systems and networks, Optics. Commun., vol. 194, no. 1-3, pp. 109-129 (2001).
22) Guan, S., et al., Modulation bandwidth enhancement and frequency chirp suppression in two-section DFB laser, J. Lightwave Technol, vol. 40, no. 22, pp. 7383-7389 (2022).
23) Matsui, Y., et al., Low-chirp isolator-free 65-GHz-bandwidth directly modulated lasers, Nature Phot., vol.15, no. 1, pp.59-63 (2021).
24) Kjebon, O., et al., 30 GHz direct modulation bandwidth in detuned loaded InGaAsP DBR lasers at 1.55 μm wavelength, Electron. Lett., vol. 33, no.6, pp. 488-489 (1997).
25) Bach, L., et al., 22-GHz modulation bandwidth of long cavity DBR laser by using a weakly laterally coupled grating fabricated by focused ion beam lithography, Phot. Technol. Lett., vol. 16, no. 1, pp. 18-20 (2004).
26) Laakso, A., Dumitrescu, M., Modified rate equation model including the photon–photon resonance, Opt. Quantum Electron., vol. 42, pp. 785-791 (2011).
27) Matsui, Y., Directly modulated laser technology: Past, present, and future, datacenter connectivity technologies. River Publishers, 2022. pp. 149-150.
28) Uddin, M., et al., High intrinsic modulation bandwidth InGaAsP/InGaAsP 1.55 μm asymmetric active multimode interferometer laser diode by using split pump configuration, J.

J. Appl. Phys., vol. 538S2, pp. 08MB09 (2014).
29) Hong, B., et al., Bandwidth enhancement scheme demonstration (from 5 GHz to 34 GHz) on direct modulation laser diode using multiple PPR (Photon-photon resonance) Active MMI, Proceedings of the 43rd European Conference and Exhibition of Optical Communications, Paper P1.SC2.22 (2017).
30) Hong, B., et al., Bandwidth enhancement scheme demonstration on direct modulation active-MMI laser diode using multiple photon photon resonance, Appl. Phys. Lett., vol. 111, no. 22, pp. 221105 (2017).
31) Xiao, H., et al., The proposal of a photon–photon resonance control scheme by using an active MMI laser diode, Photonics, vol. 10, no. 12, pp. 1298 (2023).
32) Murakami, S., et al., Observation of 60 GHz and 20 GHz multiple photon-photon resonances using active multimode interferometer laser diodes, Proceedings of 24th Microoptics Conference, pp. 304-305 (2019).
33) Iniewski, K., Integrated microsystems: electronics, photonics, and biotechnology. CRC Press. 2017, Chapter. 21, pp. 474-478.
34) Soldano, L. B., Pennings, E. C., Optical multi-mode interference devices based on self-imaging: principles and applications, J. Lightwave Technol., vol.13, no. 4, pp. 615-627 (1995).